

## Controlling Silver Ion Release of Silver Nanoparticles with Hybrid Lipid Membranes with Long-Chain Hydrophobic Thiol Anchors Decreases *in vivo* Toxicity

Arek M. Engstrom,<sup>1</sup> Henry Wu,<sup>2</sup> Marilyn R. Mackiewicz,<sup>2</sup> and Stacey L. Harper\*<sup>1,3,4</sup>

<sup>1</sup>Department of Environmental and Molecular Toxicology, Oregon State University, Corvallis, Oregon, United States; <sup>2</sup>Department of Chemistry, Portland State University, Portland, Oregon, United States; <sup>3</sup>School of Chemical, Biological, and Environmental Engineering, Oregon State University, Corvallis, Oregon, United States; <sup>4</sup>Oregon Nanoscience and Microtechnologies Institute, Corvallis, Oregon, United States

### ABSTRACT

Silver nanoparticles (AgNPs) are widely used in various commercial and industrial applications because of their antimicrobial properties. The behavior and toxicity of AgNPs are likely controlled by physicochemical properties such as size, shape, and surface chemistry; however, studies of these properties are often confounded by Ag<sup>+</sup> ion dissolution. Here a suite of spherical and triangular shaped AgNPs were prepared with increasing amounts of surface protection from their surface-coating comprising of citrate (Cit) only or a mixture of sodium oleate (SOA), phosphatidylcholine (PC), hexanethiol (HT) and propanethiol (PT) as follows: Cit, SOA-PC, SOA-PC-PT, and SOA-PC-HT. Dissolution studies showed that AgNPs with a membrane anchored by a long-chained, hydrophobic thiol in a tight packing arrangement were protected from surface oxidation and Ag<sup>+</sup> ion release, while other surface coatings did not shield the nanoparticle surface from oxidation and resulted in Ag<sup>+</sup> ion release. Embryonic zebrafish exposed to the suite of AgNPs showed low rates of mortality and morbidity to the AgNPs protected with the membrane anchored with the longest chained thiol. In contrast, AgNPs with no thiols or shorter chained thiol surface coatings allowed for increased surface oxidation and Ag<sup>+</sup> leaching that resulted in higher mortality and morbidity rates across both geometries. When the Ag<sup>+</sup> ion release was controlled, the higher surface area spherical AgNPs showed increased toxicity over the triangular AgNPs with the same surface coating. The ability to control the Ag<sup>+</sup> ion release of AgNPs provides an opportunity to understand how the physicochemical properties AgNP play a role in toxicity.

**Keywords:** silver nanoparticles, ion release, toxicity, zebrafish, lipid-membrane

Date of Submission: 29-08-2020

Date of Acceptance: 14-09-2020

### I. INTROCUCTION

Silver nanoparticles (AgNPs) are widely used due to their well understood antimicrobial properties.<sup>1-11</sup> They are utilized in a variety of consumer and commercial products, as well as industrially for wastewater treatment.<sup>12</sup> In biomedical applications, AgNPs have been used to fight HIV-1,<sup>2</sup> aid in wound care,<sup>13</sup> utilized as a antimicrobial coating in cardiac devices, catheters and surgical appliances,<sup>14</sup> and used as biosensors. The uses of AgNPs are continuously growing, as indicated by the number of patents issued involving AgNPs. From 1980 to 2010 there were 7,422 patents filed for commercial products utilizing AgNPs and 932 patents filed for consumer products utilizing AgNPs, with the US, Korea, and China being the major players in the use of both consumer

and commercial AgNP products.<sup>15</sup> Because of their high demand in a variety of fields, over 500 tons of AgNPs are manufactured annually.<sup>16</sup>

The growth in nanotechnology applications comprised of AgNPs has led to a significant interest in understanding their possible environmental and human health impacts. The diversity of commercially available AgNP products are often proprietary, not well-defined, and undergo rapid surface oxidation and dissolution of silver (Ag<sup>+</sup>) ions making their assessment difficult to study. Consequently, there is a gap in our current understanding of the relative contribution of physicochemical parameters such as shape, size, and surface coating to nanoparticle stability, nanoparticle-biological interactions (NBI), biouptake, and ecotoxicity. Current debate in the

literature over the relative influence of  $\text{Ag}^+$  to AgNP impacts needs to be directly investigated to inform risk management decisions. Most studies, thus far, have focused on the environmental and biological effect of  $\text{Ag}^+$ , which provides a baseline for the potential effects and impacts of AgNPs to organisms and ecosystems especially as AgNPs undergo dissolution to  $\text{Ag}^+$ . Thus, studies designed to evaluate the effects of AgNPs have been limited and their toxicity currently is presumably closely related to the release of  $\text{Ag}^+$ . There is a critical need to determine if the biological and environmental impacts of AgNPs are the result of its size or shape aside from its ionic constitution ( $\text{Ag}^+$ ).

Various studies have suggested that the physiochemical characteristics (size, shape, surface coating) of AgNPs play a role in uptake and toxicity. For example, smaller AgNP spheres have been shown to have increased antibacterial activity than their larger counterparts, due to increased relative surface area, allowing for greater release of  $\text{Ag}^+$ .<sup>2, 17</sup> Consequently, increased toxicity has been observed in zebrafish embryos, gills, and intestines,<sup>18-20</sup> as well as cytotoxicity in mammalian cells,<sup>21</sup> and increased acute toxicity in mice.<sup>22</sup> When looking at shape, silver nanoplates were found to have increased antibacterial activity over nanospheres and nanorods.<sup>23</sup> Silver nanoplates exhibited increased toxicity to zebrafish than nanospheres or nanowires due to surface defects that had a negative impact on cell membranes,<sup>20</sup> whereas nanospheres and nanoplates showed increased inhibition of growth of *Caenorhabditis elegans* compared to nanowires.<sup>24</sup> While these studies and others show differential toxicity based on shape of AgNPs, they are difficult to contextualize as changes to the shape of the AgNPs result in changes to other, potentially confounding properties such as size, surface area, and  $\text{Ag}^+$  dissolution. Some studies have attempted to control all nanoparticle parameters, only varying one at a time, such as shape.<sup>25-27</sup> While these studies show differential toxicity elicited by changes in physiochemical properties, they do not control for  $\text{Ag}^+$  dissolution during manufacturing, nor the continued release of  $\text{Ag}^+$  from AgNPs over time. This makes it very difficult to assess if the increased toxicity is due to the physiochemical properties of the AgNPs or  $\text{Ag}^+$  ion release.

While  $\text{Ag}^+$  ion capture agents such as cysteine,<sup>28</sup> covalent surface ligands such as Polyvinylpyrrolidone (PVP)<sup>25</sup> and Polyethylene glycol (PEG),<sup>29</sup> and aminated surface ligands with silica shells<sup>1</sup> have been applied to protect the surface to some degree from surface oxidation,  $\text{Ag}^+$  ion release is still a major interference complicating AgNP toxicity studies. The lack of well-characterized AgNP batches without major  $\text{Ag}^+$

dissolution is a major bottleneck in assessing the effects that the various physiochemical properties of AgNPs have on their fate, uptake, and toxicity. Thus, we set out to design a suite of AgNPs differentially shielded from surface oxidation and  $\text{Ag}^+$  dissolution in both spherical and triangular plate geometries. This would allow for the assessment of the effects of shape on AgNP toxicity, while simultaneously controlling and assessing confounding contribution of  $\text{Ag}^+$ . We hypothesized that hybrid lipid-coated AgNPs of both geometries with a robust coating should elicit minimal  $\text{Ag}^+$  ion release and toxicity, whereas a decrease in surface coverage should lead to a respective increase in  $\text{Ag}^+$  ion release and toxicity. Regarding shape, we hypothesized that the spherical AgNPs will have a greater toxicity due to their higher surface area to volume ratio and smaller size than the triangular AgNPs.

We created a suite of spherical (Sph) and triangular plate (Tri) AgNPs with five different surface coatings that included citrate (Cit) and a mixture of ligands that comprised of phosphatidylcholine (PC), propanethiol (PT), hexanethiol (HT), and sodium oleate (SOA). The suite of AgNPs varied in robustness based on the composition of their surface coating and can be ranked from least to most robust in the following order: Cit < SOA-PC < SOA-PC-PT < SOA-PC-HT = SOA-PC-HT (P). Dissolution studies were performed to assess the ability of the surface coating to protect the AgNP from surface oxidation and  $\text{Ag}^+$  dissolution. In addition, we assessed the toxicity of the suite of AgNPs using embryonic zebrafish (*Danio rerio*) as a model organism due to their rapid development and ease of use in nanotoxicology studies.<sup>30-36</sup> Zebrafish have very similar molecular signaling processes, cell structure, anatomy, and physiology as other higher-order vertebrates, including humans and is a good model for toxicological assessment.<sup>37-40</sup> Their rapid development and transparent body makes observing morphological and physiological malformations easy. Here the use of hybrid lipid-coated AgNPs allowed us to evaluate for the first time to the best of our knowledge the effect of AgNP size and shape on toxicity without  $\text{Ag}^+$  ions present as a confounding factor.

## II. RESULTS & DISCUSSION

### Preparation of Citrate-capped AgNPs and Hybrid Lipid AgNPs Derivatives

Here a suite of spherical and triangular AgNPs with a variety of coatings were prepared to evaluate their stability, ability to undergo surface oxidation, and toxicity. AgNPs were prepared using an established procedure with citrate as a capping

agent or hybrid lipid membrane compositions that comprised of either SOA-PC or SOA-PC-X and X (PT or HT).<sup>41</sup> The hybrid lipid membrane-coated AgNPs are similar to that previously reported of gold,<sup>42-45</sup> gold-silica core-shell,<sup>46</sup> and silica<sup>47</sup> where long-chained hydrophobic thiols are used to anchor membranes to solid supports. It is expected that AgNPs with citrate and SOA-PC will be unshielded and more susceptible to surface oxidation where  $Ag^0$  is oxidized to  $Ag^+$ , while hybrid lipid-coated AgNPs comprised of membranes that are anchored with long-chained hydrophobic thiol will be robust and shielded from surface oxidation as seen previously.<sup>41</sup> For yellow-colored citrate-capped AgNPs, a sharp and narrow localized surface plasmon resonance (LSPR) band is observed at  $\lambda_{max}$  402 nm (**Figure 1, A**). This band is characteristic of spherical AgNPs with an average diameter of  $9.30 \pm 3.58$  nm (**Figure 1, C**). In contrast, the blue-colored citrate-capped AgNPs had a somewhat broad LSPR band at  $\lambda_{max}$  742 nm (**Figure 1, B**) that indicates that there is a mixture of shapes (spheres, rods, and triangular plates) present and is consistent with that

reported previously.<sup>48</sup> The triangular plate nanoparticles have an average edge length of  $34.49 \pm 8.29$  nm (**Figure 1, D**). Upon addition of SOA there is a 2 nm red-shift in the  $\lambda_{max}$  for spherical AgNPs and a 42 nm red-shift for triangular AgNPs (**Figure 1, A and B**). This is indicative of change in the refractive index of the material upon the displacement of the citrate ligands with SOA. Upon the addition of PC and thiol (PT and HT) there is a decrease in the optical density (O.D.) and a shift in LSPR band of both spherical and triangular-shaped AgNPs (**Figure 1, A and B**). A 32 nm red-shift in the  $\lambda_{max}$  is observed for spherical AgNPs that is due to slight aggregation of the AgNPs that is more prominent when the short-chained thiol anchor, PT, is used and less prominent when the longer-chained thiol, HT, is used (**Figure 1, A**). In contrast, a 44 nm blue-shift in the  $\lambda_{max}$ , is observed with the triangular-shaped AgNPs that is due to slight etching of some of the AgNPs presents upon the addition of PT (**Figure 1, B**). No etching of the triangular-shaped SOA-PC-HT AgNPs is observed.

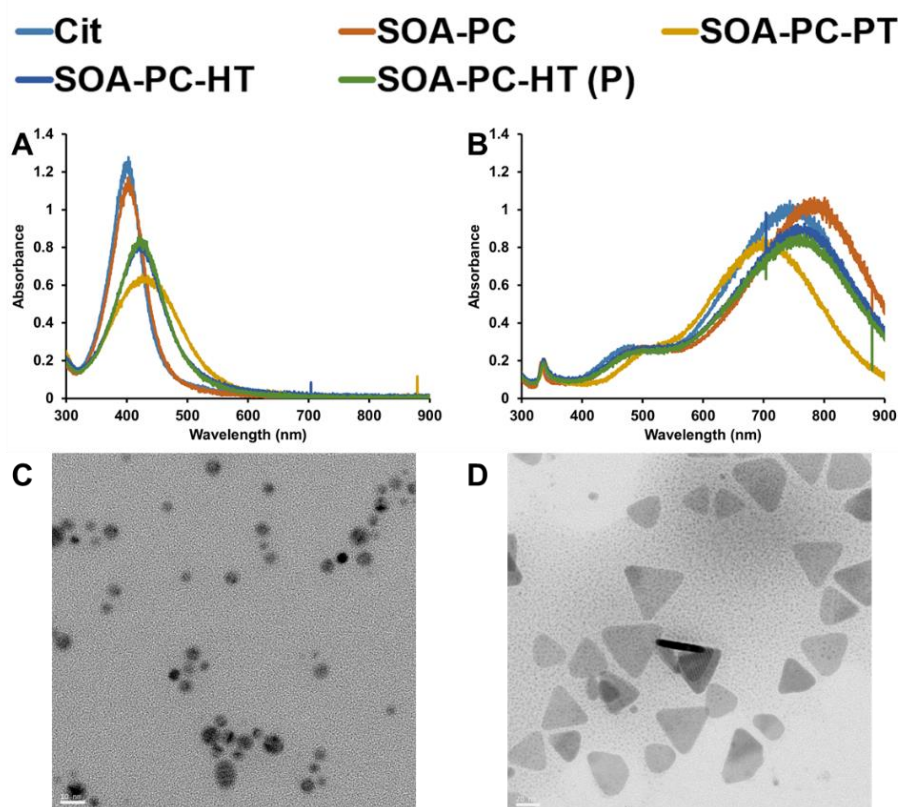


**Figure 1.** A) Representative UV-Vis spectra of A) spherical AgNPs and B) triangular-shaped AgNPs with Cit (blue), SOA-PC (orange), SOA-PC-PT (yellow), SOA-PC-HT (dark blue), and SOA-PC-HT(P) (green) in  $H_2O$ . Representative TEM micrographs of citrate-capped C) spherical AgNPs (scale bar 10 nm) and D) triangular AgNPs (scale bar 20 nm).

### Surface Oxidation Studies of Shielded and Deshielded AgNPs

The hybrid lipid-coated AgNPs with a thiol anchor are expected to be completely shielded from surface oxidation similar to hybrid lipid-coated gold nanoparticles (AuNPs) that have unique stability in the presence of strong etchants such as cyanide ( $\text{CN}^-$ ).<sup>42-45</sup> Consequently, in this study, the propensity to undergo surface oxidation of the hybrid lipid-coated AgNPs in the presence of  $\text{CN}^-$  is tested for every batch of material synthesized. These studies are important to demonstrate that the hybrid lipid membrane with a thiol anchor is completely covering the AgNP to prevent surface oxidation, allowing us to rule out the presence of  $\text{Ag}^+$  ions as a confounding factor in toxicity studies.  $\text{CN}^-$  is added

to a 1 mL sample of spherical (0.4 O.D.) or triangular (0.3 O.D.) SOA-PC-HT (P) in  $\text{H}_2\text{O}$  and the UV-Vis spectra recorded before and after incubation with  $\text{CN}^-$  for 1 h. No significant decrease in O.D. or shift in the LSPR band is observed within 1 h (**Figure 2**), 24 h, and after several weeks in the presence of  $\text{CN}^-$  indicating that the AgNPs are completely covered in a tight packing arrangement protecting the surface from etching or oxidation. Furthermore, this is consistent with previous studies of hybrid lipid-coated AuNPs and AgNPs.<sup>41-45</sup> Note: addition of  $\text{CN}^-$  to citrate-capped AgNPs degraded within minutes of addition.  $\text{CN}^-$  etch studies were performed with each batch of hybrid lipid-coated AgNPs and before any toxicity or stability studies.

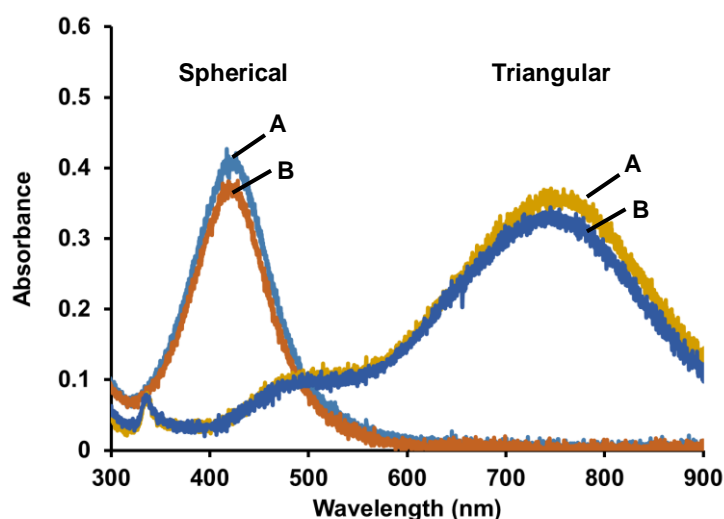


**Figure 2.** Representative UV-Vis spectra of spherical and triangular SOA-PC-HT (P) AgNPs a) before and b) 1 h after the addition 20  $\mu\text{L}$  of 307 mM KCN.

### Stability Studies of Shielded and Unshielded AgNPs in FW

To evaluate the long-term stability the various AgNP platforms are exposed to the same conditions used for evaluating their toxicity in fish water (FW) over a 1-month period. Briefly, 1 mL samples of spherical and triangular-shaped AgNPs in FW (1:2 ratio of AgNP to FW) are retrieved and UV-Vis spectra are collected at each time point (initial, 1 day, and 1, 2, 3, and 4 weeks). The UV-Vis spectra of the spherical AgNPs showed significant changes in the LSPR band and O.D. overtime for all AgNP types except for the robustly shielded SOA-PC-HT and SOA-PC-HT(P) nanoparticles that are also stable in the presence of  $\text{CN}^-$  (**Figure 2**). The spherical citrate-capped AgNPs are the least stable and showed the greatest change within the first 24 h with a 50% reduction in O.D. and color. Within 1 week there is a considerable loss of color and drop

in O.D. indicating that the citrate-capped AgNPs underwent rapid  $\text{Ag}^+$  ion dissolution (**Figure 3, A & Figure S1**). The UV-Vis spectra of the spherical SOA-PC and SOA-PC-PT AgNPs show a much slower decrease in the O.D. over a month indicating that the SOA-PC and SOA-PC-PT coating offers some protection of surface oxidation over time (**Figure 2, B and C**). In addition to partial surface oxidation, the SOA-PC-PT also aggregated over time as evident by the visual sedimentation of AgNPs (**Figure S1**). The most protection is offered to the SOA-PC-HT and SOA-PC-HT (P), where no change in O.D. (**Figure 2, D and E**) or color is observed over 1 month (**Figure S1**). From this study it was found that the spherical AgNPs can be ranked in the order of increasing stability where  $\text{Cit} < \text{SOA-PC} \approx \text{SOA-PC-PT} < \text{SOA-PC-HT} = \text{SOA-PC-HT(P)}$ .

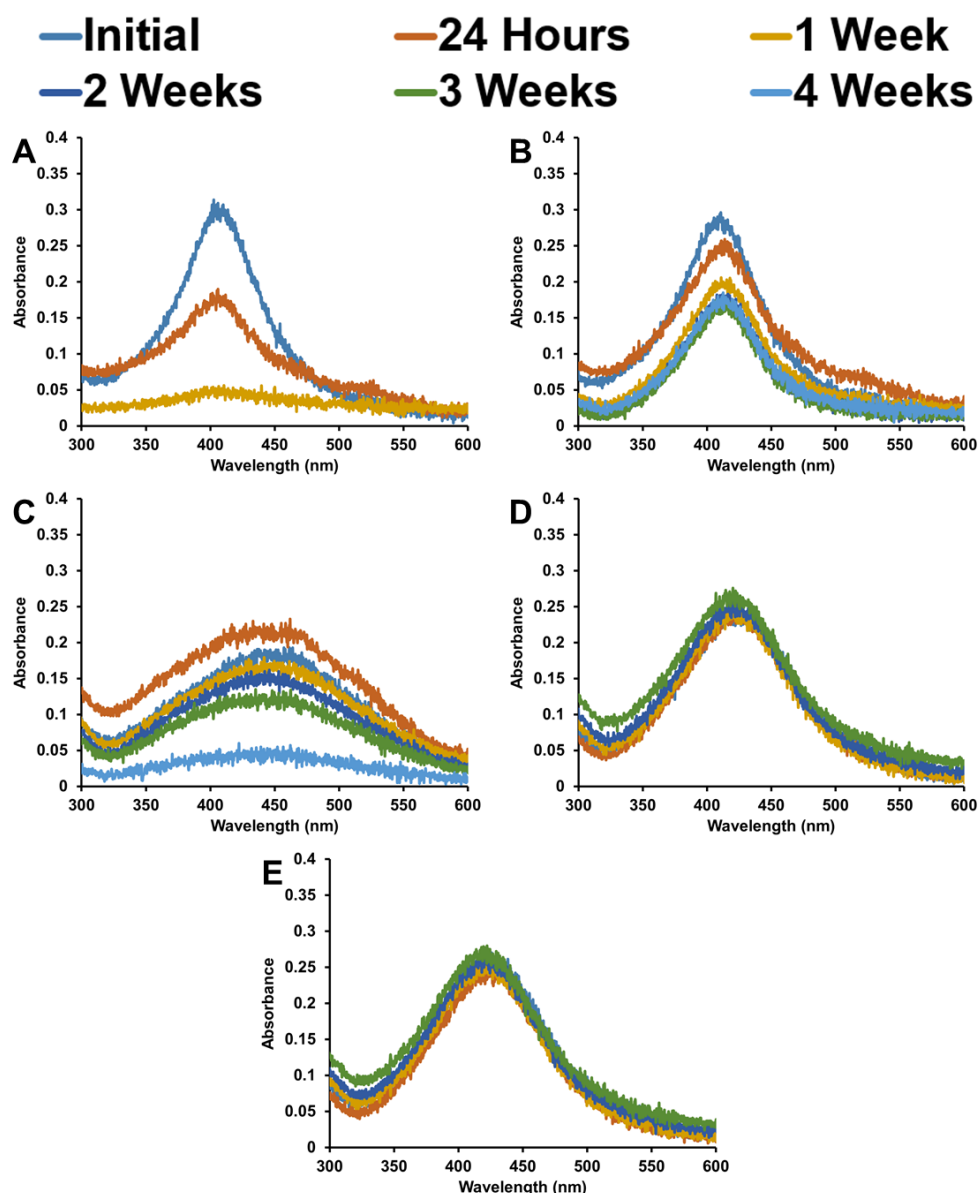


**Figure 2.** Representative UV-vis spectra of spherical a) Cit, b) SOA-PC, c) SOA-PC-PT, d) SOA-PC-HT, e) SOA-PC-HT(P) in the presence of FW (1:2 ratio of AgNP to FW) at pH 7.4 from 0 h (blue), 1 day (orange), 1 week (yellow), 2 weeks (dark blue), 3 weeks green), and 4 weeks (light blue).

Interestingly, more significant changes are observed with the triangular-shaped AgNPs derivatives. The addition of FW to the citrate-capped AgNPs leads to rapid conversion of triangular to spherical AgNPs as indicated by an immediate change in color from blue to green as well as the appearance of an intense and sharp LSPR band at  $\lambda_{\max}$  395 nm (Figure 3, A). Similarly, with the SOA-PC AgNPs there is a rise of an LSPR band at  $\lambda_{\max}$  460 nm indicating these AgNPs undergo a partial conversion of triangular-shaped AgNPs to spherical AgNPs that remains stable over a month (Figure 3, B). In both cases the full or partial conversion occurs because of the presence of Cl<sup>-</sup>

ions that attack the high-energy points on the triangular-shaped AgNPs to etch them into other shapes. The UV-Vis spectra of SOA-PC-PT show a significant decrease in the O.D. after 1 week (Figure 3, C) and upon visual inspection, aggregation is observed (Figure S1). A similar decrease in O.D. (Figure 3, D) and evidence of precipitation in FW (Figure S1) is observed with SOA-PC-HT AgNPs. Not surprisingly, there is no change in the O.D. of the SOA-PC-HT (P) AgNPs that are found to be extremely stable in FW with no aggregation. It is surprising that the unpurified hybrid lipid-coated Ag-Cit-SOA-PC-HT nanoparticles aggregated (Figure S1) and is likely the result of nanoparticle-

nanoparticle interactions from the presence of excess citrate ligands and lipids. The triangular-shaped AgNPs can be ranked in the order of

increasing stability where Cit < SOA-PC ≈ SOA-PC-PT < SOA-PC-HT < SOA-PC-HT(P).

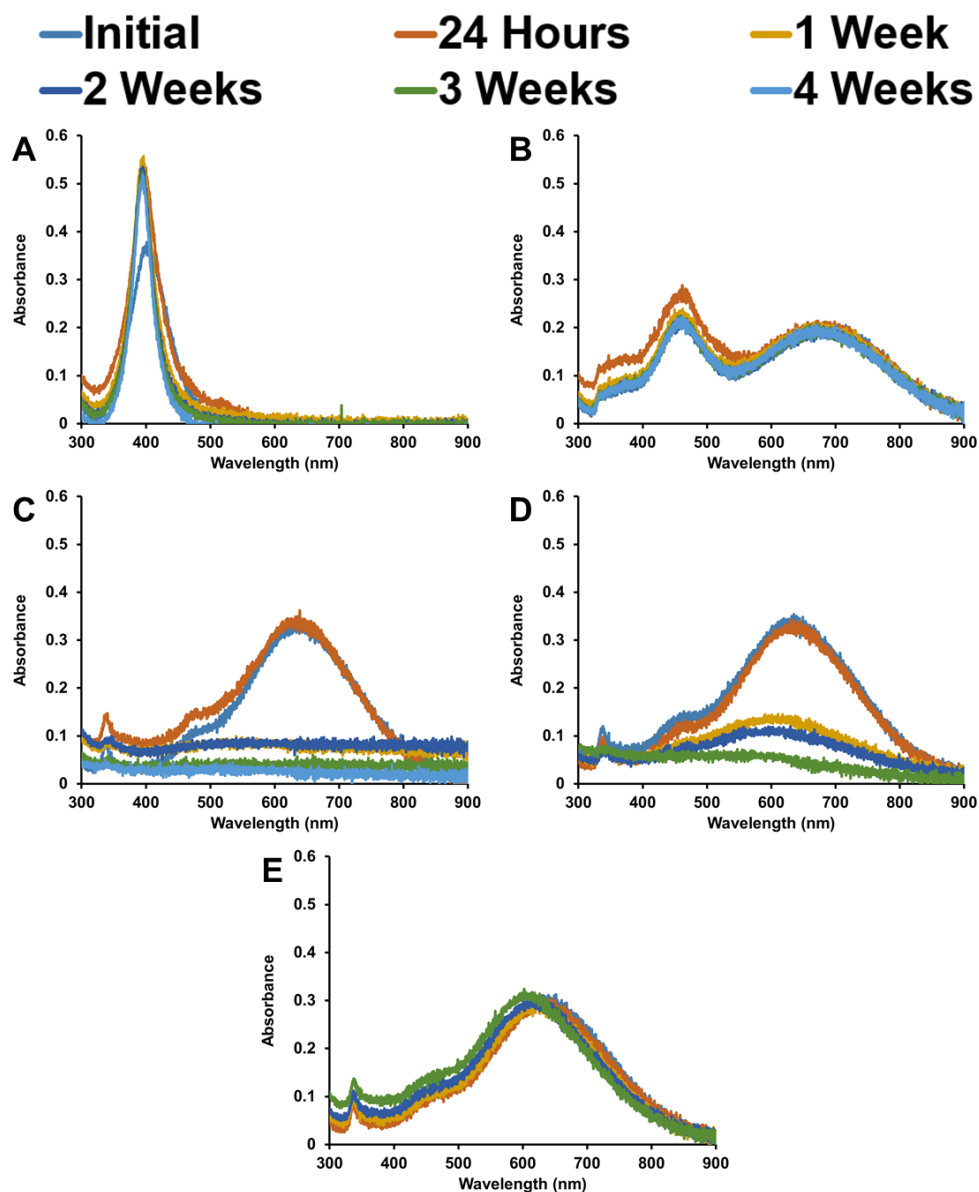


**Figure 3.** Representative UV-vis spectra of triangular A) Cit, B) SOA-PC, C) SOA-PC-PT, D) SOA-PC-HT, E) SOA-PC-HT(P) AgNPs in the presence of FW (1:2 ratio of AgNP to FW) at pH 7.4 from 0 h (black), 1 day (orange), 1 week (yellow), 2 weeks (dark blue), 3 weeks (green), and 4 weeks (light blue).

#### Quantifying Ag<sup>+</sup> Release from AgNPs by ICP-MS

To further elucidate the cause of the changes observed in the O.D. and  $\lambda_{\max}$  of the LSPR band of the spherical and triangular-shaped AgNPs in the presence of FW, ICP-MS studies are performed. More specifically, ICP-MS is used to monitor Ag<sup>+</sup> ion release from the AgNPs over time in FW. Briefly, 1 mL samples of the spherical and triangular-shaped AgNPs in FW (1:2 ratio of AgNP to FW) are retrieved and centrifuged with a Vivaspin

concentration with a MWCO of 3kDa to separate the AgNPs from Ag<sup>+</sup> ions in the filtrate. Filtrates were collected initially (0 h), at 1 day, and weeks 1, 2, 3, and 4 for ICP-MS analysis. The ICP-MS analysis of filtrate of spherical AgNPs show increased concentrations of Ag<sup>+</sup> ions for the citrate-capped and SOA-PC AgNPs, with the greatest concentrations released within 24 h followed by a decrease over time. In contrast, the level of Ag<sup>+</sup> ions are below the detection limit for SOA-PC-PT, SOA-PC-HT, and

SOA-PC-HT(P) (**Figure 4, A**). This indicates that minimal  $\text{Ag}^+$  ions are released from the hybrid lipid-coated AgNPs that are completely shielded from surface oxidation and confirms that the decrease in stability observed for SOA-PC-PT AgNPs is due to aggregation (**Figure 2, C**). Similarly, the highest level of  $\text{Ag}^+$  ion concentration is observed for the

triangular-shaped Ag-Cit and Ag-Cit-SOA-PC within 1 h followed by a decrease over time (**Figure 4, B**). No detectable  $\text{Ag}^+$  ion levels are observed for the triangular-shaped AgNPs coated with SOA-PC-PT, SOA-PC-HT, and SOA-PC-HT(P) (**Figure 4, B**).

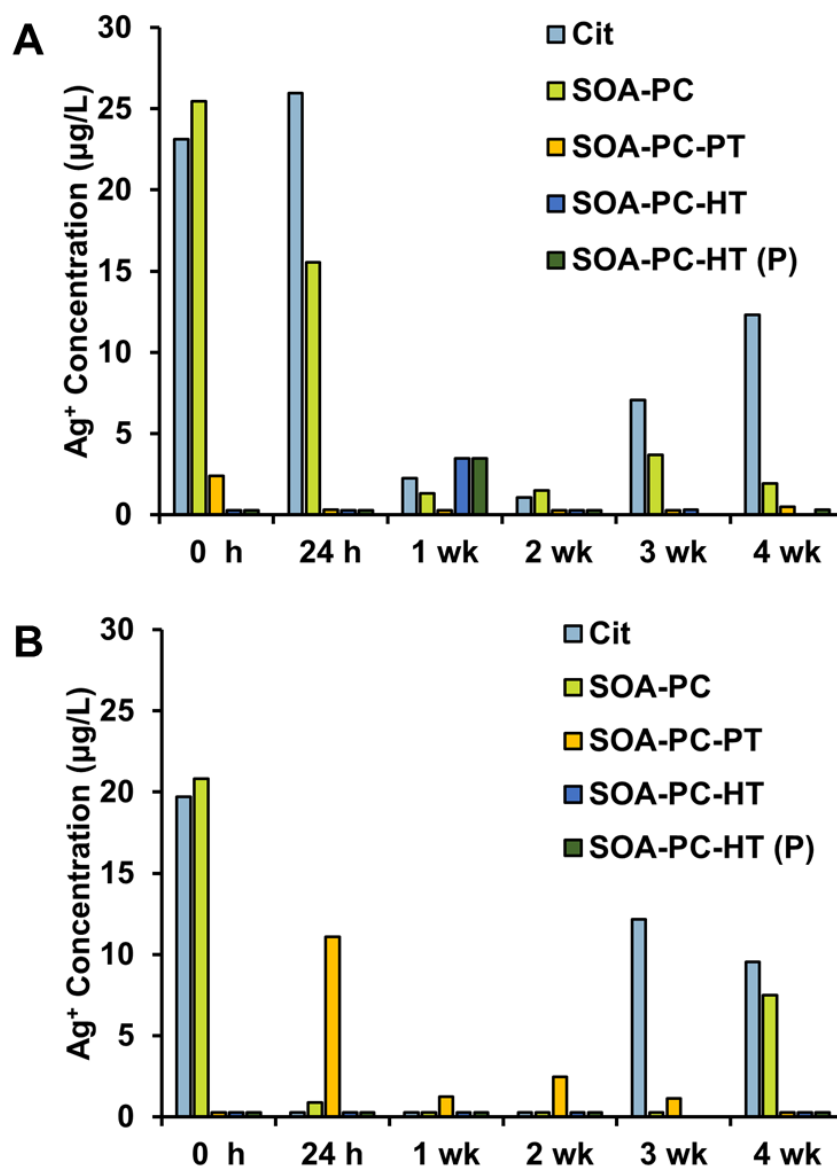


**Figure 4.** ICP-MS analysis of A) spherical and B) triangular AgNPs in the presence of FW (1:2 ratio of AgNPs to FW) from the initial (0 h), 24 hours, 1 week, 2 weeks, 3 weeks, and 4 weeks.

#### TEM Characterization of Purified Hybrid Lipid-coated AgNPs

Since the purified spherical and triangular-shaped hybrid lipid-coated AgNPs (**Figure 6, A and B**) show minimal  $\text{Ag}^+$  ion release overtime in FW, TEM studies were done to confirm the that

nanoparticles did not change shape or size. Samples of spherical and triangular-shaped SOA-PC-HT (P) AgNPs are cast onto a TEM grid at 1 h, 1 week, and 4 weeks and imaged. The sizes of the spherical and triangular-shaped SOA-PC-HT (P) AgNPs remained unchanged at each of the timepoints

imaged (**Figure 6**) and the shapes remained comparable to the sizes of the stock solution (**Figure 1, C and D**). The diameter of the spherical AgNPs at week 4 was  $9.69 \pm 2.08$  nm compared to the spherical stock at  $9.30 \pm 3.58$  nm. The triangular-shaped AgNPs had an edge length of  $35.06 \pm 4.11$

nm, whereas the stock solution is  $34.50 \pm 8.30$  nm. TEM imaging confirmed the results observed by UV-Vis and ICP-MS, that the SOA-PC-HT (P) does not undergo any significant changes in size or morphology because they are completely protected from surface oxidation.

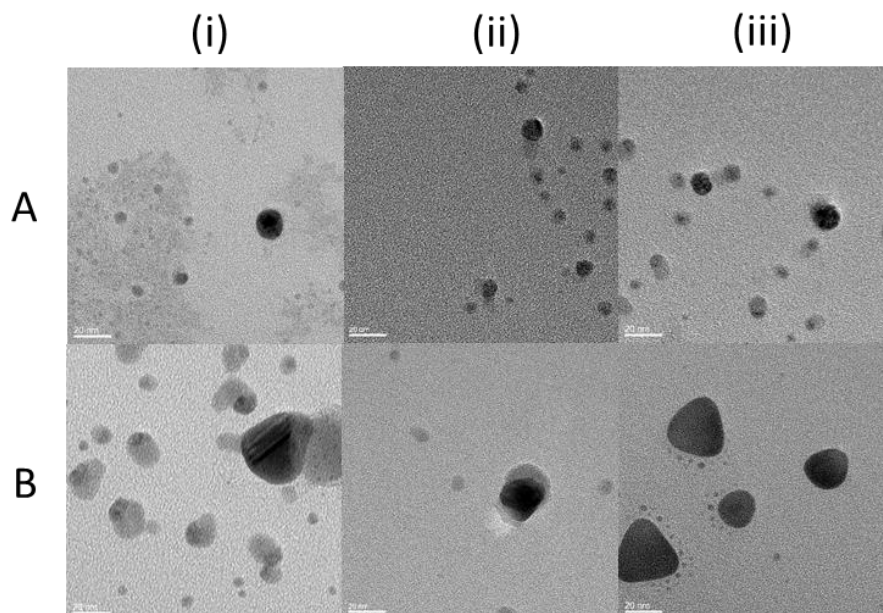


**Figure 5.** Representative TEM images of the both A) spherical and B) triangular AgNPs coated with SOA-PC-HT(P) after 1 hour (i), 1 week (ii), and 4 weeks (iii).

### Toxicity Testing

To evaluate the toxicity of the AgNP suite, embryonic zebrafish were exposed to each of the ten AgNPs at concentrations ranging from 0.03125 mg Ag/L and 4 mg Ag/L for 120 h and observed at 24 hours post fertilization (hpf) and 120 hpf for the suite of end points previously described. Mortality at 120 hpf decreased as the amount of surface protection on the AgNP increased (**Figure 6**). The spherical citrate-capped and SOA-PCAgNPs elicited the highest mortality, with significant mortality observed at 0.5 mg Ag/L and 100% mortality at 4 mg Ag/L. The lowest mortality is observed with the spherical and triangular-shaped SOA-PC-HT AgNPs, showing no significant

mortality across any of the concentrations tested. When AgNPs with the most robust surface coating were purified (SOA-PC-HT (P)), removing free ligands, a slight increase in toxicity is observed; both the spherical and triangular-shaped SOA-PC-HT (P) AgNPs show significant mortality at the highest concentration tested (4 mg Ag/L). This increased toxicity upon purification is likely due to increased uptake facilitated by a less negative surface charge. Toxicity data show both a decrease in toxicity associated with an increase in complexity of surface coating and a decrease in toxicity of the triangular-shaped AgNPs (**Figure 6, B**) compared to the spherical AgNPs with the same surface coating (**Figure 6, A**).

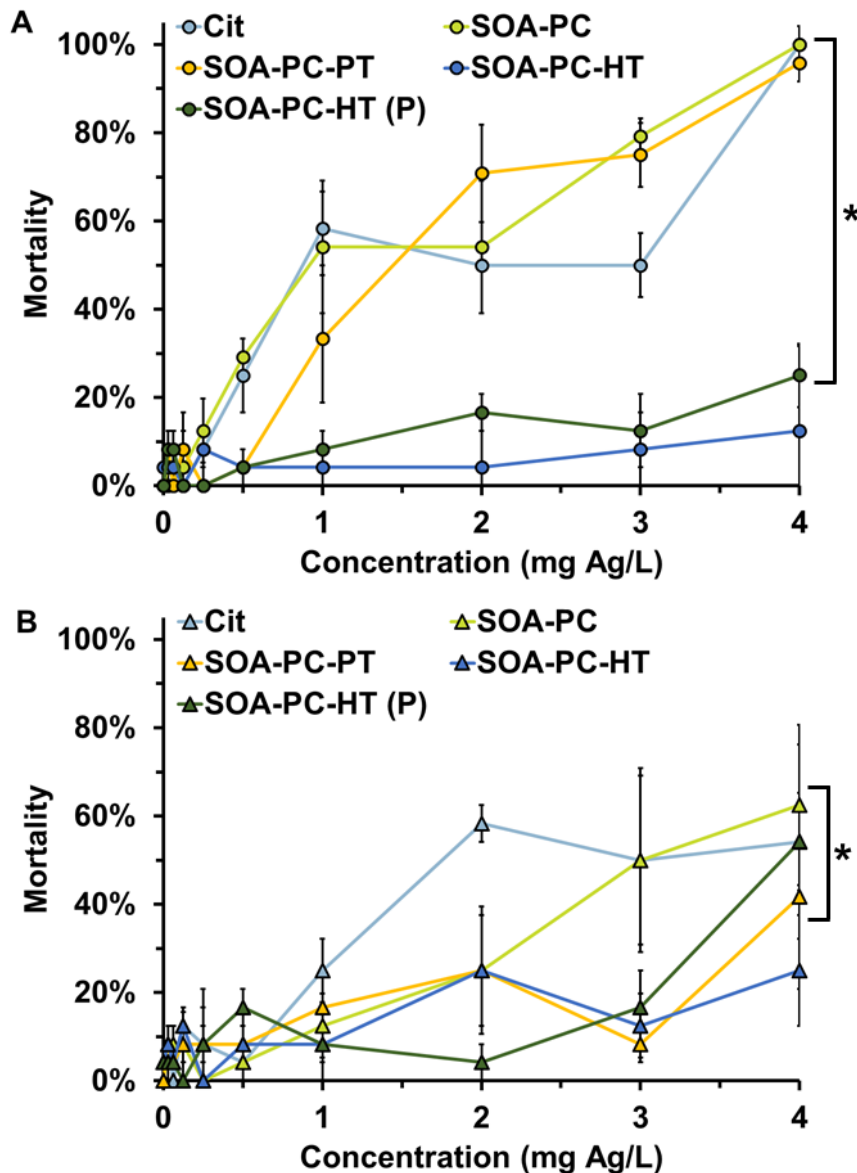


**Figure 6.** Concentration-response curves of zebrafish mortality at 120 hpf exposed to A) spherical AgNPs and B) triangular AgNPs. This data represents three experimental replicates of  $n = 8$  for a total of  $n = 24$  for each exposure condition. \* Indicates significant difference from control ( $p$ -value  $< 0.05$ ).

Aside from increased mortality, the spherical AgNPs also generally caused increases in sublethal malformations of the zebrafish (Table 1). Lowest observable effect levels (LOEL) were determined to be the concentration where a significant number of fishes are affected by a given malformation, as calculated by a Fisher's Exact Test ( $p < 0.05$ ). Significant occurrences of pericardial edema (PE), yolk sack edema (YSE), and jaw malformations are observed in fish exposed to both spherical and triangular-shaped AgNPs regardless of surface coating. Pericardial edema is swelling of the heart and cardiac area, whereas yolk sack edema is swelling of the yolk sack and surrounding area

(Figure S3, B and C). Both are likely caused by ionic changes in the media during the embryo's development. More interestingly, a small, but significant, number of jaw malformations occurred in both the spherical citrate-capped and SOA-PC AgNPs. Jaw malformations are a much less common developmental malformation and are most likely due to the AgNP causing an adverse effect during the developmental window of formation of the jaw (Figure S3, C).

**Table 1.** Sublethal effects of AgNP suit observed at 120 hpf indicates significant occurrence of jaw malformations (Jaw), pericardial edema (PE), and yolk sack edema (YSE). This data represents three experimental replicates of  $n = 8$  for a total of  $n = 24$  for each exposure condition.

Spherical AgNPs	Lowest Observable Effect Level			Increasing Amount of AgNP Shielding	Triangular AgNPs	Lowest Observable Effect Level		
	Jaw	PE	YSE			Jaw	PE	YSE
Cit	2 mg Ag/L	0.5 mg Ag/L	0.5 mg Ag/L	↓	Cit	-	2 mg Ag/L	2 mg Ag/L
SOA-PC	3 mg Ag/L	1 mg Ag/L	0.5 mg Ag/L		SOA-PC	-	2 mg Ag/L	2 mg Ag/L
SOA-PC-PT	-	0.5 mg Ag/L	0.5 mg Ag/L		SOA-PC-PT	-	3 mg Ag/L	3 mg Ag/L
SOA-PC-HT	-	-	4 mg Ag/L		SOA-PC-HT	-	-	4 mg Ag/L
SOA-PC-HT (P)	-	4 mg Ag/L	3 mg Ag/L		SOA-PC-HT (P)	-	3 mg Ag/L	2 mg Ag/L

The AgNPs with coatings that shielded the AgNPs from surface oxidation showed decreased toxicity, supporting our hypothesis that AgNPs shielded from surface oxidation and  $Ag^+$  ion release (as demonstrated by UV-Vis, ICP-MS, and TEM) are biocompatible. Sublethal malformations observed are consistent with the literature showing the tendency of AgNPs to accumulate in various tissues (gills, intestines, and muscles) within the zebrafish resulting in sublethal toxicity.<sup>18</sup> Amongst these malformations, edema of the pericardium and yolk sack are common<sup>1,49</sup> and likely due to the ionic changes created by the dissolution of the  $Ag^+$  ions.<sup>50</sup> Jaw malformations are a more rare morphological malformation, however, have been seen in previous AgNP studies.<sup>1,51</sup> The jaw and head of the zebrafish are particularly vulnerable to nanoparticle effects as they are primarily cartilage allowing for smaller nanoparticles to have more pronounced effects on their development.<sup>52</sup> When comparing the relative toxicity of these malformations, Harper *et al.* proposed an embryonic zebrafish metric (EZ Metric) to compare both the mortality and morbidity observed in embryonic zebrafish development.<sup>30</sup> This metric assigned various weights to each malformation based on the impact of the given sublethal malformation. Under this metric mortality at 24 hpf is weighted at a 1.0, mortality at 120 hpf is weighted at a 0.95, pericardial edema is weighted as a 0.12, yolk sack edema is weighted as a 0.1, and malformations to the jaw are weighted as a 0.04.<sup>30</sup> Using this combined measure of mortality and morbidity to compare the toxicity of the AgNPs, two distinct trends arise: 1) general decrease in toxicity in both the spherical and triangular-shaped AgNPs as the coating completely shields the AgNPs to prevent surface oxidation and  $Ag^+$  ion release; and 2) distinctly lower toxicity of the triangular-shaped AgNPs when compared with the spherical AgNPs with the same surface coating (Table 2).

The combined mortality and morbidity analysis along with normalized dissolution data confirms what has been shown in previous studies on AgNPs;  $Ag^+$  dissolution is one of the driving mechanisms behind AgNP toxicity. Our studies demonstrate that the release of  $Ag^+$  ions is closely related to the toxicity of the AgNP suite. Comparing total dissolution over the first week to the Lowest Observable Adverse Effect Level (LOAEL) of the zebrafish in the same time frame, a direct relationship between  $Ag^+$  ion release and toxicity is observed (Table 2). The pattern of decreasing toxicity with increasing shielding of the AgNPs with the hybrid membrane coating are observed across both the spherical and triangular geometries, indicating that  $Ag^+$  ion release is likely the main cause of toxicity regardless of particle shape.

**Table 2.** Summary of dissolution and toxicity for spherical and triangular AgNPs used to assess risk to zebrafish.

Spherical AgNPs	Total Dissolution at 1 Week	LOAEL	Increasing Amount of AgNP Shielding	Triangular AgNPs	Total Dissolution at 1 Week	LOAEL
Cit	7.34%	0.5 mg Ag/L		Cit	2.58%	2 mg Ag/L
SOA-PC	5.68%	0.5 mg Ag/L		SOA-PC	3.05%	2 mg Ag/L
SOA-PC-PT	0.52%	0.5 mg Ag/L		SOA-PC-PT	2.17%	3 mg Ag/L
SOA-PC-HT	0.07%	4 mg Ag/L		SOA-PC-HT	0.09%	4 mg Ag/L
SOA-PC-HT (P)	0.07%	3 mg Ag/L		SOA-PC-HT (P)	0.08%	2 mg Ag/L

### III. CONCLUSION

In summary, we have shown for the first-time toxicity studies on AgNPs with surface coatings that provide protection from surface oxidation and Ag<sup>+</sup> dissolution, a confounding factor in other AgNP toxicity studies. When AgNPs are completely shielded with a protective hybrid lipid membrane anchored by a long-chained hydrophobic thiol, Ag<sup>+</sup> dissolution and the toxicity of the AgNPs is minimal as demonstrated by the spherical and triangular-shaped SOA-PC-HT (P) AgNPs in this study. In comparison to the other, less robust, surface coatings the hybrid lipid-coated AgNPs showed minimal release of Ag<sup>+</sup> ions and minimal change in shape or morphology over a month leading to minimal toxicity. With hybrid lipid-coated AgNPs we were able to show that spherical nanoparticles with high surface area were more toxic compared to triangular-shaped AgNPs. This preliminary study with hybrid lipid-coated AgNPs also represents the first direct observation of the effect of size and shape on toxicity and opens the door for many other studies where the effect of size, shape, and surface area can be fully interrogated in the absence of Ag<sup>+</sup> ions. These studies will allow us to evaluate and elucidate the contribution of the physiological parameters that play a role in nanoparticle-biological interactions, toxicity, stability, and biouptake. Further toxicological studies will allow us to inform policy makers through risk assessment. Lastly, the ability to tune AgNPs to control their lease of Ag<sup>+</sup> and decrease toxicity is useful in improving the shelf-life of commercial AgNP antimicrobials and for controlling Ag<sup>+</sup> ion release over time in medical devices such as stents and other implanted devices. The ability to control Ag<sup>+</sup> ion release will revolutionize the use and study of AgNPs across the nanotechnology field.

### IV. METHODS AND MATERIALS

#### Reagents

Trisodium citrate dihydrate 99% (Na<sub>3</sub>C<sub>6</sub>H<sub>3</sub>O<sub>7</sub>), 1-hexanethiol 95% (CH<sub>3</sub>(CH<sub>2</sub>)<sub>4</sub>CH<sub>2</sub>SH), 1-propanethiol 99% (CH<sub>3</sub>CH<sub>2</sub>CH<sub>2</sub>SH), chloroform, pronase (from *Streptomyces griseus*) were purchased from Sigma Aldrich. Silver nitrate 98% (AgNO<sub>3</sub>) was purchased from G. Frederick Smith Chemical Company (GFS). Hydrogen peroxide 30% (H<sub>2</sub>O<sub>2</sub>) and sodium borohydride 99% (NaBH<sub>4</sub>) were obtained from VWR Chemicals. L- $\alpha$ -phosphatidylcholine was purchased from Avanti Lipids. Sodium Oleate 97% was from Tokyo Chemical Industry Co, Ltd. 10 mM sodium phosphate buffer was prepared for PC suspension at pH 8. Instant Ocean Salts were purchased from Aquatic Ecosystems. Nanopure water was from a Milli-Q ultrapure system. All chemicals were used as received.

#### Synthesis of Citrate-capped Silver Nanoparticles

The synthesis of AgNPs was modified from a similar procedure.<sup>48</sup> Briefly, in a 125 mL Erlenmeyer flask, AgNO<sub>3</sub> (43 mL of 0.109 mM in H<sub>2</sub>O) was combined with H<sub>2</sub>O<sub>2</sub> (120  $\mu$ L of 30% w/w) and trisodium citrate dihydrate (3.68 mL of 34.32 mM in H<sub>2</sub>O). The reaction mixture was allowed to stir for approximately 1 minute at 600 RPM with a magnetic stir bar. A freshly prepared aqueous solution of NaBH<sub>4</sub> (220  $\mu$ L of 100 mM in H<sub>2</sub>O) was rapidly added to the mixture the center of the vortex. After NaBH<sub>4</sub> addition, over 2-3 min, the solution undergoes a rapid color change from yellow to orange, then followed by red to purple, and then stabilizes at a blue color that is indicative of triangular-shaped AgNPs. Spherical AgNPs were prepared in a same fashion with the NaBH<sub>4</sub> volume reduced to 100  $\mu$ L followed by 5  $\mu$ L drops until the color stabilizes at a golden yellow. All AgNP solutions were stirred for an additional 10 min before storing overnight in a refrigerator at 4 °C and filtered with a 0.2  $\mu$ m polytetrafluoroethylene(PTFE) filter before studies.

The spherical and triangular-shaped AgNPs had a  $\lambda_{\max}$  at 402 nm and 738 nm in H<sub>2</sub>O, respectively.

### Synthesis of AgNPs with Various Surface Coatings

Hybrid lipid-coated AgNPs was previously described.<sup>41</sup> Both spherical and triangular-shaped citrate-capped AgNPs were diluted to a final maximum optical density of 1.2 and 0.8 respectively. To form the Ag-SOA-PC nanoparticles, 1 mL of citrate-capped AgNPs was placed in a 5 mL scintillation vial and SOA (1.1  $\mu$ L, 9.4 mM in H<sub>2</sub>O) was added. The AgNP-SOA solution was vortexed for 5 sec and allowed to incubate at room temperature for 20 min. This was followed by the addition of PC liposomes (10.4  $\mu$ L, 0.32 mM in 10 mM sodium phosphate buffer at pH 8) that was vortexed for 5 sec and incubated for 40 min at room temperature to form Ag-SOA-PC nanoparticles. To form the Ag-SOA-PC-PT and Ag-SOA-PC-HT nanoparticles, 1.4  $\mu$ L of thiol was added to 1 mL of Ag-SOA-PC, either PT (30 mM in ethanol) or HT (30 mM in ethanol) respectively. The Ag-SOA-PC-thiol (PT or HT) solution was vortexed for 5 sec and allowed to incubate at room temperature for at least 30 min before use. The Ag-SOA-PC-HT nanoparticles was further purified by incubating the AgNPs with 10 mM Tween20 (20  $\mu$ L per mL of AgNPs) to remove "nanoparticle-free" liposomes followed by ultracentrifugation (4700 rpm for 4 min) using a Vivaspin column with a molecular weight cut off (MWCO) of 10 kDa. The AgNPs were washed with 6x with 15 mL of H<sub>2</sub>O and resuspended back to the same starting volume to yield Ag-SOA-PC-HT (P). Both spherical and triangular AgNPs were prepared with the following compositions: Cit, SOA-PC, SOA-PC-PT, SOA-PC-HT, and SOA-PC-HT (P).

### Stability and Ag<sup>+</sup> Release Studies with AgNPs

To determine if the hybrid lipid-coated AgNPs were shielded from oxidation, a well-known cyanide (CN<sup>-</sup>) etch test was performed.<sup>53</sup> CN<sup>-</sup> is used to oxidize metals such as Au<sup>0</sup> and Ag<sup>0</sup> to Au<sup>III</sup> or Ag<sup>I</sup> in the presence of O<sub>2</sub>. An 800  $\mu$ L solution of a 1:1 ratio of AgNPs with an optical density (O.D.) of 0.4 in H<sub>2</sub>O was incubated with 20  $\mu$ L of 307 mM KCN in a 5 mL scintillation vial for 1 h. The UV-Vis spectra were collected before and after the addition of KCN and the change in the O.D. and  $\lambda_{\max}$  monitored.

To evaluate the differential release rate of Ag<sup>+</sup> ions in the presence of fish water (FW) AgNPs samples in H<sub>2</sub>O were diluted 1:2 ratio of AgNPs to FW and stored at room temperature for 1 month in the dark at 25°C. FW was prepared by mixing 0.26 g/L Instant Ocean salts in deionized water and

adjusting the pH with sodium bicarbonate to 7.2  $\pm$  0.2. Conductivity was verified to be between 480-520  $\mu$ S/cm. From these samples, 1 mL aliquots of AgNPs were retrieved and centrifuged using a Vivaspin column with a MWCO of 3 kDa. Samples were centrifuged at 4700 rpm for 4 min and the filtrates collected for ICP-MS analysis. The UV-Vis spectra were collected overtime and the change in the O.D. as well as  $\lambda_{\max}$  monitored.

### ICP-MS Studies

Samples of AgNPs (1:9 ratio of AgNPs and H<sub>2</sub>O) were prepared. ICP-MS analysis of the AgNPs were conducted at the Elemental Analysis Core at Oregon Health Sciences University (OHSU). The samples were further diluted by a dilution factor of 6.05 with 1% HNO<sub>3</sub> (trace metal grade, Fisher) into 15 mL acid-rinsed centrifuge tubes (10  $\mu$ L of the sample was added to 1000  $\mu$ L 1% HNO<sub>3</sub>). The obtained data were quantified using a 10-point (0, 0.5, 1, 2, 5, 10, 20, 50, 100, 500 ng/g, ppb) calibration curve using a multi-element standard (VHG-SM70B-100) for Fe, Cu, Zn, and Ag. Samples were run in triplicate studies and data were averaged. A coefficient of variance (CoV) was determined from frequent measurements of a sample containing ~10 ppb of the multi-element standard (VHG-SM70B-100). An internal standard (Sc, Ge, Bi) was continuously introduced with the sample was used to correct for detector fluctuations and to monitor plasma stability. Elemental recovery was evaluated by measuring a NIST reference material (water, SRM 1643f) and found to be >90 % for all determined elements.

### Transmission Electron Microscopy (TEM) and UV-Vis Spectroscopy

Samples were prepared by drop-casting dilute solutions of AgNPs onto carbon-coated (300 Å) Formvar films on copper grids (Ted Pella). Samples sat for 5 min before excess sample is wicked off by with a piece of filter paper and the process was repeated 3 times. Transmission electron micrographs were acquired on a Tecnai F-20 FEI microscope using a CCD detector at an acceleration voltage of 200 kV. AgNP size analysis was performed using ImageJ Software. Absorbance measurements were performed with an Ocean Optics USB2000 UV-visible spectrophotometer using a 1.0 cm path length quartz cell.

### Characterization of AgNPs in Exposure Media

All zebrafish experiments were carried out in FW, so the inter-laboratory characterization of the AgNPs was done in FW as well. Each AgNP was characterized as synthesized using a Malvern Zetasizer Nano. Hydrodynamic diameter (HDD)

and zeta potential were measured for each AgNP. HDD estimates the agglomerate size in the given media, and zeta potential (ZP) approximates the AgNPs surface charge relative to the media. Summary of HDD and ZP measurements can be found in **Table S1**.

### Toxicity Testing

Adult zebrafish (*Danio rerio*) were maintained at Oregon State University's Sinnhuber Aquatic Research Laboratory (SARL) in a water flow-through system under standard laboratory conditions: constant temperature of 28 °C under a 14:10 hour light-dark cycle.<sup>54</sup> Embryos were collected and staged from group spawns of wild-type tropical 5D zebrafish. Staging is important to ensure that all embryos are at the same developmental stage at the start of each experiment.<sup>55</sup> Embryos were enzymatically dechorionated at 6 hpf using pronase following the procedure of Usenko *et. al.*<sup>56</sup> Removal of the chorion is critical as the chorion has been shown to protect the embryo from exposure, serving as a physical barrier and sink for nanomaterials and other chemicals.<sup>57, 58</sup> At 8 hpf, the dechorionated embryos were individually exposed to 200 µL of AgNP suspensions varying from 0.03125 mg Ag/L to 4 mg Ag/L in FW in clear, flat bottom 96-well plates ( $n = 24$  per concentration). All exposure concentrations of AgNPs were normalized based on mass of silver, allowing for the isolation of shape and surface coating as the variables of interest. Zebrafish exposure solutions of AgNPs were made by diluting the stock solutions of AgNPs in FW and then briefly vortexing. Plates were then incubated at 26.9 °C under a 14:10 hour light-dark cycle.

At 24 hpf, embryos were observed, using a dissecting microscope, for mortality, developmental progression, notochord malformations, and presence of spontaneous movement. Spontaneous movement is a behavioral end point described by Kimmel *et. al.* as "rhythmic bouts of swimming."<sup>55</sup> At 120 hpf, embryos were again observed for mortality along with a suite of other physiological, behavioral, and morphological endpoints. The endpoints assessed at 120 hpf include: malformations of the body axis, brain, eye, caudal fin, pectoral fin, jaw, otic, altered pigmentation, snout, swim bladder, and somites; edema of the yolk sack and pericardium; alterations to circulation; and changes in behavioral response to touch. In this study, the most observed sub-lethal malformations were pericardial edema, yolk sack edema, and malformations of the jaw. All experiments were performed in compliance with national care and use guidelines and approved by the Institutional Animal Care and Use Committee (IACUC) at Oregon State University.

### Statistical Analyses

Statistical analyses were performed using Sigma Plot 13.0. Fisher's exact test was used to compare specific developmental endpoints between treatment and controls in the embryonic zebrafish assay. Analysis of variance (ANOVA) was used to evaluate differences among treatment groups across equivalent concentrations. Differences were considered statistically significant at  $p \leq 0.05$  for all analyses.

### AUTHOR CONTRIBUTIONS

The manuscript was written through contributions of all authors. All authors have given approval to the final version of the manuscript.

### ASSOCIATED CONTENT

The following files are available free of charge. Images of AgNPs at various timepoints, images of representative zebrafish malformations, and hydrodynamic diameter and zeta potential measurements of AgNPs in exposure media. (Supplemental Figures.pdf)

### FUNDING SOURCES

This work was supported by NSF Grant #1762245.

### ABBREVIATIONS

AgNP, silver nanoparticle; Cit, citrate; SOA, sodium oleate; PC, phosphatidylcholine; HT, hexanethiol; PT, propanethiol; NBI, nanoparticle-biological interactions; Ag<sup>+</sup>, silver ions; PVP, polyvinylpyrrolidone; PEG, polyethylene glycol; LSPR, localized surface plasmon resonance; O.D., optical density; AuNP, gold nanoparticle; CN<sup>-</sup>, cyanide; FW, fish water; PE, pericardial edema; YSE yolk sac edema; LOEL, lowest observable effect level; LOAEL; lowest observable adverse effect level; hpf, hours post fertilization; MWCO, molecular weight cutoff; HDD, hydrodynamic diameter; ZP, zeta potential.

## REFERENCES

1. Bonventre, J. A.; Pryor, J. B.; Harper, B. J.; Harper, S. L., The impact of aminated surface ligands and silica shells on the stability, uptake, and toxicity of engineered silver nanoparticles. *Journal of Nanoparticle Research* **2014**, *16* (12), 2761.
2. Elechiguerra, J. L.; Burt, J. L.; Morones, J. R.; Camacho-Bragado, A.; Gao, X.; Lara, H. H.; Yacaman, M. J., Interaction of silver nanoparticles with HIV-1. *Journal of nanobiotechnology* **2005**, *3* (1), 6.
3. Feng, Q. L.; Wu, J.; Chen, G. Q.; Cui, F. Z.; Kim, T. N.; Kim, J. O., A mechanistic study of the antibacterial effect of silver ions on *Escherichia coli* and *Staphylococcus aureus*. *Journal of Biomedical Materials Research* **2000**, *52*, 662-668.
4. Ivask, A.; ElBadawy, A.; Kaweeteerawat, C.; Boren, D.; Fischer, H.; Ji, Z.; Chang, C. H.; Liu, R.; Tolaymat, T.; Telesca, D.; Zink, J. I.; Cohen, Y.; Holden, P. A.; Godwin, H. A., Toxicity mechanisms in *Escherichia coli* vary for silver nanoparticles and differ from ionic silver. *ACS Nano* **2014**, *8* (1), 374-386.
5. Morones, J. R.; Elechiguerra, J. L.; Camacho, A.; Holt, K.; Kouri, J. B.; Ramírez, J. T.; Yacaman, M. J., The bactericidal effect of silver nanoparticles. *Nanotechnology* **2005**, *16* (10), 2346.
6. Panacek, A.; Kvitek, L.; Pucek, R.; Kolar, M.; Vecerova, R.; Pizurova, N.; Sharma, V. K.; Nevecna, T. j.; Zboril, R., Silver Colloid Nanoparticles: Synthesis, Characterization, and Their Antibacterial Activity. *J. Phys. Chem. B* **2006**, *110* (33), 16248-16253.
7. Rai, M. K.; Deshmukh, S. D.; Ingle, A. P.; Gade, A. K., Silver nanoparticles: the powerful nanoweapon against multidrug-resistant bacteria. *J. Appl. Microbiol.* **2012**, *112* (5), 841-852.
8. Shrivastava, S.; Bera, T.; Roy, A.; Singh, G.; Ramachandrarao, P.; Dash, D., Characterization of enhanced antibacterial effects of novel silver nanoparticles. *Nanotechnology* **2007**, *18* (22), 225103/1-225103/9.
9. Sondi, I.; Salopek-Sondi, B., Silver nanoparticles as antimicrobial agent: A case study on *E. coli* as a model for Gram-negative bacteria. *J. Colloid Interface Sci.* **2004**, *275* (1), 177-182.
10. Wu, F.; Harper, B. J.; Harper, S. L., Differential dissolution and toxicity of surface functionalized silver nanoparticles in small-scale microcosms: impacts of community complexity. *Environmental Science: Nano* **2017**, *4* (2), 359-372.
11. Xiu, Z.-m.; Zhang, Q.-b.; Puppala, H. L.; Colvin, V. L.; Alvarez, P. J. J., Negligible Particle-Specific Antibacterial Activity of Silver Nanoparticles. *Nano Lett.* **2012**, *12* (8), 4271-4275.
12. Liang, Z.; Das, A.; Hu, Z., Bacterial response to a shock load of nanosilver in an activated sludge treatment system. *Water Research* **2010**, *44* (18), 5432-5438.
13. Rigo, C.; Ferroni, L.; Tocco, I.; Roman, M.; Munivrana, I.; Gardin, C.; Cairns, W. R. L.; Vindigni, V.; Azzena, B.; Barbante, C.; Zavan, B., Active silver nanoparticles for wound healing. *Int. J. Mol. Sci.* **2013**, *14*, 4817-4840.
14. Lansdown, A. B., Silver in health care: antimicrobial effects and safety in use. *Curr Probl Dermatol* **2006**, *33*, 17-34.
15. Lem, K. W.; Choudhury, A.; Lakhani, A. A.; Kuyate, P.; Haw, J. R.; Lee, D. S.; Iqbal, Z.; Brumlik, C. J., Use of nanosilver in consumer products. *Recent Pat Nanotechnol* **2012**, *6* (1), 60-72.
16. Mueller, N. C.; Nowack, B., Exposure Modeling of Engineered Nanoparticles in the Environment. *Environmental Science & Technology* **2008**, *42* (12), 4447-4453.
17. Morones, J. R.; Elechiguerra, J. L.; Camacho, A.; Holt, K.; Kouri, J. B.; Ramírez, J. T.; Yacaman, M. J., The bactericidal effect of silver nanoparticles. *Nanotechnology* **2005**, *16* (10), 2346-2353.
18. Liu, H.; Wang, X.; Wu, Y.; Hou, J.; Zhang, S.; Zhou, N.; Wang, X., Toxicity responses of different organs of zebrafish (*Danio rerio*) to silver nanoparticles with different particle sizes and surface coatings. *Environmental Pollution* **2019**, *246*, 414-422.
19. Kim, K.-T.; Truong, L.; Wehmas, L.; Tanguay, R. L., Silver nanoparticle toxicity in the embryonic zebrafish is governed by particle dispersion and ionic environment. *Nanotechnology* **2013**, *24* (11), 115101.
20. George, S.; Lin, S.; Ji, Z.; Thomas, C. R.; Li, L.; Mecklenburg, M.; Meng, H.; Wang, X.; Zhang, H.; Xia, T.; Hohman, J. N.; Lin, S.; Zink, J. I.; Weiss, P. S.; Nel, A. E., Surface defects on plate-shaped silver nanoparticles contribute to its hazard potential in a fish gill cell line and zebrafish embryos. *ACS Nano* **2012**, *6* (5), 3745-59.
21. Park, M. V.; Neigh, A. M.; Vermeulen, J. P.; de la Fonteyne, L. J.; Verharen, H. W.; Briedé, J. J.; van Loveren, H.; de Jong, W. H., The effect of particle size on the cytotoxicity, inflammation, developmental toxicity and genotoxicity of silver nanoparticles. *Biomaterials* **2011**, *32* (36), 9810-9817.
22. Cho, Y.-M.; Mizuta, Y.; Akagi, J.-i.; Toyoda, T.; Sone, M.; Ogawa, K., Size-dependent acute toxicity of silver nanoparticles in mice. *Journal of Toxicologic Pathology* **2018**, *31* (1), 73-80.
23. Pal, S.; Tak, Y. K.; Song, J. M., Does the antibacterial activity of silver nanoparticles depend on the shape of the nanoparticle? A study of the

gram-negative bacterium *Escherichia coli*. *Appl. Environ. Microbiol.* **2007**, 73 (6), 1712-1720.

24. Moon, J.; Kwak, J. I.; An, Y.-J., The effects of silver nanomaterial shape and size on toxicity to *Caenorhabditis elegans* in soil media. *Chemosphere* **2019**, 215, 50-56.

25. Gorka, D. E.; Osterberg, J. S.; Gwin, C. A.; Colman, B. P.; Meyer, J. N.; Bernhardt, E. S.; Gunsch, C. K.; DiGulio, R. T.; Liu, J., Reducing Environmental Toxicity of Silver Nanoparticles through Shape Control. *Environmental Science & Technology* **2015**, 49 (16), 10093-10098.

26. Li, Y.; Kroger, M.; Liu, W. K., Shape effect in cellular uptake of PEGylated nanoparticles: comparison between sphere, rod, cube and disk. *Nanoscale* **2015**, 7 (40), 16631-46.

27. Tree-Udom, T.; Seemork, J.; Shigyou, K.; Hamada, T.; Sangphech, N.; Palaga, T.; Insin, N.; Pan-In, P.; Wanichwecharungruang, S., Shape Effect on Particle-Lipid Bilayer Membrane Association, Cellular Uptake, and Cytotoxicity. *ACS Applied Materials & Interfaces* **2015**, 7 (43), 23993-24000.

28. Piccapietra, F.; Allué, C. G.; Sigg, L.; Behra, R., Intracellular Silver Accumulation in *Chlamydomonas reinhardtii* upon Exposure to Carbonate Coated Silver Nanoparticles and Silver Nitrate. *Environmental Science & Technology* **2012**, 46 (13), 7390-7397.

29. Liu, C.; Leng, W.; Vikesland, P. J., Controlled Evaluation of the Impacts of Surface Coatings on Silver Nanoparticle Dissolution Rates. *Environmental Science & Technology* **2018**, 52 (5), 2726-2734.

30. Harper, B.; Thomas, D.; Chikkagoudar, S.; Baker, N.; Tang, K.; Heredia-Langner, A.; Lins, R.; Harper, S., Comparative hazard analysis and toxicological modeling of diverse nanomaterials using the embryonic zebrafish (EZ) metric of toxicity. *Journal of Nanoparticle Research* **2015**, 17 (6), 250.

31. Harper, S.; Usenko, C.; Hutchison, J.; Maddux, B.; Tanguay, R., In vivo biodistribution and toxicity depends on nanomaterial composition, size, surface functionalisation and route of exposure. *Journal of Experimental Nanoscience* **2008**, 3 (3), 195-206.

32. Harper, S. L.; Carriere, J. L.; Miller, J. M.; Hutchison, J. E.; Maddux, B. L. S.; Tanguay, R. L., Systematic Evaluation of Nanomaterial Toxicity: Utility of Standardized Materials and Rapid Assays. *ACS Nano* **2011**, 5 (6), 4688-4697.

33. Harper, S. L.; Dahl, J. A.; Maddux, B. L.; Tanguay, R. L.; Hutchison, J. E., Proactively designing nanomaterials to enhance performance and minimise hazard. *International Journal of Nanotechnology* **2008**, 5 (1), 124-142.

34. Lin, S.; Zhao, Y.; Ji, Z.; Ear, J.; Chang, C. H.; Zhang, H.; Low-Kam, C.; Yamada, K.; Meng, H.; Wang, X.; Liu, R.; Pokhrel, S.; Mädler, L.; Damoiseaux, R.; Xia, T.; Godwin, H. A.; Lin, S.; Nel, A. E., Zebrafish High-Throughput Screening to Study the Impact of Dissolvable Metal Oxide Nanoparticles on the Hatching Enzyme, ZHE1. *Small* **2013**, 9 (9-10), 1776-1785.

35. Lin, S.; Zhao, Y.; Nel, A. E.; Lin, S., Zebrafish: An In Vivo Model for Nano EHS Studies. *Small* **2013**, 9 (9-10), 1608-1618.

36. Lee, K. J.; Nallathambiy, P. D.; Browning, L. M.; Osgood, C. J.; Xu, X.-H. N., In Vivo Imaging of Transport and Biocompatibility of Single Silver Nanoparticles in Early Development of Zebrafish Embryos. *ACS Nano* **2007**, 1 (2), 133-143.

37. Hill, A. J.; Teraoka, H.; Heideman, W.; Peterson, R. E., Zebrafish as a Model Vertebrate for Investigating Chemical Toxicity. *Toxicological Sciences* **2005**, 86 (1), 6-19.

38. Howe, K.; Clark, M. D.; Torroja, C. F.; Torrance, J.; Berthelot, C.; Muffato, M.; Collins, J. E.; Humphray, S.; McLaren, K.; Matthews, L.; McLaren, S.; Sealy, I.; Caccamo, M.; Churcher, C.; Scott, C.; Barrett, J. C.; Koch, R.; Rauch, G. J.; White, S.; Chow, W.; Kilian, B.; Quintais, L. T.; Guerra-Assuncao, J. A.; Zhou, Y.; Gu, Y.; Yen, J.; Vogel, J. H.; Eyre, T.; Redmond, S.; Banerjee, R.; Chi, J.; Fu, B.; Langley, E.; Maguire, S. F.; Laird, G. K.; Lloyd, D.; Kenyon, E.; Donaldson, S.; Sehra, H.; Almeida-King, J.; Loveland, J.; Trevanion, S.; Jones, M.; Quail, M.; Willey, D.; Hunt, A.; Burton, J.; Sims, S.; McLay, K.; Plumb, B.; Davis, J.; Clee, C.; Oliver, K.; Clark, R.; Riddle, C.; Elliot, D.; Threadgold, G.; Harden, G.; Ware, D.; Begum, S.; Mortimore, B.; Kerry, G.; Heath, P.; Phillimore, B.; Tracey, A.; Corby, N.; Dunn, M.; Johnson, C.; Wood, J.; Clark, S.; Pelan, S.; Griffiths, G.; Smith, M.; Glithero, R.; Howden, P.; Barker, N.; Lloyd, C.; Stevens, C.; Harley, J.; Holt, K.; Panagiotidis, G.; Lovell, J.; Beasley, H.; Henderson, C.; Gordon, D.; Auger, K.; Wright, D.; Collins, J.; Raisen, C.; Dyer, L.; Leung, K.; Robertson, L.; Ambridge, K.; Leongamornlert, D.; McGuire, S.; Gilderthorp, R.; Griffiths, C.; Manthavadi, D.; Nichol, S.; Barker, G.; Whitehead, S.; Kay, M.; Brown, J.; Murnane, C.; Gray, E.; Humphries, M.; Sycamore, N.; Barker, D.; Saunders, D.; Wallis, J.; Babbage, A.; Hammond, S.; Mashreghi-Mohammadi, M.; Barr, L.; Martin, S.; Wray, P.; Ellington, A.; Matthews, N.; Ellwood, M.; Woodmansey, R.; Clark, G.; Cooper, J.; Tromans, A.; Grafham, D.; Skuce, C.; Pandian, R.; Andrews, R.; Harrison, E.; Kimberley, A.; Garnett, J.; Fosker, N.; Hall, R.; Garner, P.; Kelly, D.; Bird, C.; Palmer, S.; Gehring, I.; Berger, A.; Dooley, C. M.; Ersan-Urun, Z.; Eser, C.; Geiger, H.; Geisler, M.; Karotki, L.; Kirn, A.; Konantz, J.; Konantz, M.;

- Oberlander, M.; Rudolph-Geiger, S.; Teucke, M.; Lanz, C.; Raddatz, G.; Osoegawa, K.; Zhu, B.; Rapp, A.; Widaa, S.; Langford, C.; Yang, F.; Schuster, S. C.; Carter, N. P.; Harrow, J.; Ning, Z.; Herrero, J.; Searle, S. M.; Enright, A.; Geisler, R.; Plasterk, R. H.; Lee, C.; Westerfield, M.; de Jong, P. J.; Zon, L. I.; Postlethwait, J. H.; Nusslein-Volhard, C.; Hubbard, T. J.; Roest Crollius, H.; Rogers, J.; Stemple, D. L., The zebrafish reference genome sequence and its relationship to the human genome. *Nature* **2013**, *496* (7446), 498-503.
39. Tropepe, V.; Sive, H. L., Can zebrafish be used as a model to study the neurodevelopmental causes of autism? *Genes, brain, and behavior* **2003**, *2* (5), 268-81.
40. Zon, L. I.; Peterson, R. T., In vivo drug discovery in the zebrafish. *Nature reviews. Drug discovery* **2005**, *4* (1), 35-44.
41. Miesen, T. J. F., D, C.; Ajarapu, R.; Mackiewicz, M. R., "Shape-locked" Hybrid Lipid-coated Silver Nanoparticles: Control of Silver Ion Dissolution. *RSC Advances* **2020**, *10* (27), 15677-15693.
42. Mackiewicz, M. R.; Hodges, H. L.; Reed, S. M., C-Reactive Protein Induced Rearrangement of Phosphatidylcholine on Nanoparticle Mimics of Lipoprotein Particles. *The Journal of Physical Chemistry B* **2010**, *114* (16), 5556-5562.
43. Sitaula, S.; Mackiewicz, M. R.; Reed, S. M., Gold nanoparticles become stable to cyanide etch when coated with hybrid lipid bilayers. *Chemical Communications* **2008**, (26), 3013-3015.
44. Wang, M. S.; Messersmith, R. E.; Reed, S. M., Membrane curvature recognition by C-reactive protein using lipoprotein mimics. *Soft Matter* **2012**, *8* (30), 7909-7918.
45. Orendorff, C. J.; Murphy, C. J., Quantitation of Metal Content in the Silver-Assisted Growth of Gold Nanorods. *The Journal of Physical Chemistry B* **2006**, *110* (9), 3990-3994.
46. Levin, C. S.; Kundu, J.; Janesko, B. G.; Scuseria, G. E.; Raphael, R. M.; Halas, N. J., Interactions of Ibuprofen with Hybrid Lipid Bilayers Probed by Complementary Surface-Enhanced Vibrational Spectroscopies. *The Journal of Physical Chemistry B* **2008**, *112* (45), 14168-14175.
47. Piper-Feldkamp, A. R.; Wegner, M.; Brzezinski, P.; Reed, S. M., Mixtures of Supported and Hybrid Lipid Membranes on Heterogeneously Modified Silica Nanoparticles. *The Journal of Physical Chemistry B* **2013**, *117* (7), 2113-2122.
48. Huang, T.; Xu, X.-H. N., Synthesis and characterization of tunable rainbow colored colloidal silver nanoparticles using single-nanoparticle plasmonic microscopy and spectroscopy. *Journal of Materials Chemistry* **2010**, *20* (44), 9867-9876.
49. Asharani, P.; Wu, Y. L.; Gong, Z.; Valiyaveetil, S., Toxicity of silver nanoparticles in zebrafish models. *Nanotechnology* **2008**, *19* (25), 255102.
50. Rider, S. A.; Tucker, C. S.; del-Pozo, J.; Rose, K. N.; MacRae, C. A.; Bailey, M. A.; Mullins, J. J., Techniques for the in vivo assessment of cardio-renal function in zebrafish (*Danio rerio*) larvae. *The Journal of physiology* **2012**, *590* (8), 1803-1809.
51. Bar-Ilan, O.; Albrecht, R. M.; Fako, V. E.; Furgeson, D. Y., Toxicity assessments of multisized gold and silver nanoparticles in zebrafish embryos. *Small* **2009**, *5* (16), 1897-1910.
52. Xue, J. Y.; Li, X.; Sun, M. Z.; Wang, Y. P.; Wu, M.; Zhang, C. Y.; Wang, Y. N.; Liu, B.; Zhang, Y. S.; Zhao, X., An assessment of the impact of SiO<sub>2</sub> nanoparticles of different sizes on the rest/wake behavior and the developmental profile of zebrafish larvae. *Small* **2013**, *9* (18), 3161-3168.
53. Hajizadeh, S.; Farhadi, K.; Forough, M.; Sabzi, R. E., Silver nanoparticles as a cyanide colorimetric sensor in aqueous media. *Analytical Methods* **2011**, *3* (11), 2599-2603.
54. Westerfield, M., The zebrafish book: a guide for the laboratory use of zebrafish. [http://zfin.org/zf\\_info/zfbook/zfbk.html](http://zfin.org/zf_info/zfbook/zfbk.html) **2000**.
55. Kimmel, C. B.; Ballard, W. W.; Kimmel, S. R.; Ullmann, B.; Schilling, T. F., Stages of embryonic development of the zebrafish. *Developmental dynamics : an official publication of the American Association of Anatomists* **1995**, *203* (3), 253-310.
56. Usenko, C. Y.; Harper, S. L.; Tanguay, R. L., Fullerene C60 exposure elicits an oxidative stress response in embryonic zebrafish. *Toxicology and Applied Pharmacology* **2008**, *229* (1), 44-55.
57. Henn, K.; Braunbeck, T., Dechoriation as a tool to improve the fish embryo toxicity test (FET) with the zebrafish (*Danio rerio*). *Comparative Biochemistry and Physiology Part C: Toxicology & Pharmacology* **2011**, *153* (1), 91-98.
58. Kim, K.-T.; Tanguay, R. L., The role of chorion on toxicity of silver nanoparticles in the embryonic zebrafish assay. *Environ Health Toxicol* **2014**, *29* (0), e2014021-0.